1-2015

The Future of Carbon-Based Scaffolds in Foot and Ankle Surgery

Jarema S. Czarnecki
University of Dayton, jczarnecki1@udayton.edu

Khalid Lafdi
University of Dayton, klafdi1@udayton.edu

Panagiotis A. Tsonis
University of Dayton, ptsonis1@udayton.edu

The Future of Carbon-Based Scaffolds in Foot and Ankle Surgery

Khalid Lafdi, DSc, PhD[a,*], Jarema S. Czarnecki, MS, PhD[b], Panagiotis A. Tsonis, PhD[c]

KEYWORDS

• Biomaterials • Carbon • Scaffolds • Reconstruction • Tissue • Cell growth • Biomechanics • Biologics

KEY POINTS

- Carbon-based materials offer enhanced biological response and tunability.
- Carbon-based scaffolds offer tensile properties comparable with those of current synthetic tissue scaffolds.
- Cellular behavior on carbon-based scaffolds is enhanced by varying material orientation, porosity, and crystallinity.

INTRODUCTION

Autologous grafts have been the gold standard in tissue replacement and the most accurate means of recapitulating both the biological and mechanical properties of tissue. However, autologous grafts have had complications and drawbacks. Skin grafting, a prime example of an autologous tissue graft, has been limited by the size of graft, availability, and secondary donor site morbidity.[1] Use of cadaveric tissues circumvents several limitations of autologous grafts; however, sterilization processes used to reduce the risk of disease transmission potentially weaken tissues and eliminate living cells and some growth factors from scaffolds, making them suboptimal tissue

Disclosure Statement: There are no commercial relationships to products of companies mentioned in the article. The funding for this article was provided by University of Dayton and Center for Tissue Regeneration and Engineering at Dayton (TREND). The authors do not have any corporate appointments related to the products or companies mentioned in this article. The authors do not have any financial relationships to products mentioned in this article.

[a] Chemical and Materials Engineering, University of Dayton, 300 College Park, Dayton, OH 45469-0240, USA; [b] Department of Mechanical Engineering, University of Dayton, 300 College Park, Dayton, OH 45469, USA; [c] Biology, Center for Tissue Regeneration and Engineering (TREND), University of Dayton, 300 College Park, Dayton, OH 45469, USA
* Corresponding author.
E-mail address: klafdi1@udayton.edu

Clin Podiatr Med Surg ■ (2014) ■–■
http://dx.doi.org/10.1016/j.cpm.2014.09.001 podiatric.theclinics.com
0891-8422/14/$ – see front matter

replacements.[2,3] Chemical cross-linkage of tissue scaffolds has been used in some circumstances to strengthen weak tissues, but can result in a prolonged inflammatory response and limit graft integration in vivo.[4–9] Partial enzymatic digestion of cadaveric tissues has also been used to improve graft porosity, which potentially assists with graft neovascularization, although this procedure has not been overwhelmingly successful.[8] Proprietary methods of chemically and physically stripping tissues of cellular materials have been commercially developed to minimize graft rejection and loss of essential biological factors; however, these methods cannot be universally applied to all tissues.[6,10] GraftJacket Matrix (GJ) (Wright Medical, Arlington, TN, USA),[4] an acellular human dermis–derived graft, is an example of a commercially available graft that is commonly used in surgery for soft-tissue augmentation and repair.[4,10–13] The elastic properties of skin-derived scaffolds make GJ an inferior replacement for stiffer tissues such as tendon. Hence, current limitations in tissue processing have spawned interest in emerging technologies that enable precise engineering and manufacturing of scaffold materials on a nanoscale that recapitulate the unique mechanical needs of a variety of tissues while promoting tissue repair that also occurs on a nanoscale.

To date, biomedical scaffold materials have included synthetic, semisynthetic, and tissue-derived matrices with or without biological activity from growth factors or living cells incorporated within the scaffolds.[10,14–19] Various extracellular matrix molecules such as collagen and resorbable synthetic materials commonly utilized in suture and medical implants have all been used as scaffolds in the past.[16,18,20,21] The most advanced generations of commercially available scaffolds attempt to provide some level of structural function with biological activity, such as Trinity (Orthofix, Lewisville, TX, USA),[22] which combines mesenchymal stem cells with a cancellous bone allograft and is used for bone healing; Infuse (Medtronic, Minneapolis, MN, USA),[23] which incorporates recombinant bone morphogenic protein 2 with a resorbable collagen scaffold sponge and is used in spine fusion; Apligraf (Organogenesis, Canton, MA, USA),[24] which integrates human keratinocytes and dermal fibroblasts with bovine type I collagen as a graft for the treatment of skin ulcerations; and GraftJacket Matrix,[4] an acellular human dermis–derived scaffold with retained growth factors and extracellular matrix molecules.

Carbon-based materials are novel subsets of synthetic materials that have been incorporated into medical scaffolds, implants, and nanoartifact drug-delivery vehicles because of their strength, flexibility, durability, and biocompatibility, but have been examined less extensively as a combined vehicle for cell delivery and biomechanical construct for soft-tissue repair and regeneration.[25–30] Potential advantages of an engineered carbon scaffold may include the following: (1) tunable geometric and surface characteristics to fit biological demands of a healing tissue; (2) reproducible mechanical properties to meet specific functional requirements; (3) lack of donor site morbidity; (4) no communicable disease transmission; and (5) unlimited availability.

This article examines the mechanical behavior of 2 fibrous carbon-based scaffolds and evaluates their potential as a vehicle for cell and biologics delivery that promotes tissue repair. The structure, tensile properties, and human fibroblast adhesion and proliferation on carbon scaffold substrates were analyzed and compared with a control scaffold, GJ, which is commonly used in surgery for soft-tissue augmentation and repair.[4,6,10,11,13,31,32]

MATERIALS AND METHODS

Materials

A spool of commercially available PAN-based carbon fibers from Cytec Industries Inc. (Woodland Park, NJ, USA) was used to create carbon scaffold substrates. Before

scaffold preparation, carbon fibers were heat treated at 150°C for 30 minutes and milled to 5-mm size. A 1% (weight/volume) poly(ε-caprolactone)/acetone solvent was added to form a slurry. The slurry was cast in a mold and evaporated to leave behind a veil scaffold (labeled CV1 and CV2, n = 10 per group). Unidirectional carbon laminate was made by aligning unidirectional P120 carbon tow fabric (labeled CF1 and CF2, n = 10 per group). Samples were ultrasonicated and sterilized in 100% ethanol for 1 hour. GraftJacket Matrix (labeled GJ, n = 20) was donated by Wright Medical Technology Inc (Arlington, TN).

Environmental Scanning Electron Microscopy of Scaffolds

Environmental scanning electron microscopy (ESEM) was used to examine geometric properties of scaffolds. A Hitachi ESEM device (Hitachi, Schaumburg, IL, USA) was used to visualize the microscale surface of scaffolds. Samples were imaged at 500×.

Micro–Computed Tomography of Scaffolds

Micro–computed tomography (μCT; Scanco Medical, Wayne, PA, USA) was used to analyze scaffold porosity, pore size, and scaffold geometry. Samples were analyzed before mechanical testing and culture. Samples were scanned at a resolution of 7 μm/slice. Sample porosity was calculated with proprietary software provided by Scanco Medical.

Mechanical Characterization of Scaffolds

Tensile properties of scaffolds were examined using an MTS mechanical tester (MTS, Eden Prairie, MN, USA). Grip fixtures were used to secure samples and prevent sample tearing. All scaffolds were hydrated when tested under tension, as GJ function in vivo is under hydrated conditions. Hydration of GJ and carbon scaffolds was performed according to manufacturers' instructions for GJ hydration. Ten samples for each scaffold group were analyzed at 25.4 mm/min. Stress and strain data were recorded. The slope of the linear region of the stress-strain curve was used to determine the elastic modulus. For this study, the strain region between 0% and 3% was considered low strain, for comparison of carbon-based scaffolds with GJ control.

Fibroblast Culture on Scaffolds

Human dermal fibroblasts (ATCC CRL2703, Manassas, VA, USA) were cultured in flasks with Dulbecco F12 medium (DMEM; Gibco BRL, Invitrogen, Carlsbad, CA, USA) supplemented with 10% fetal bovine serum (FBS; Atlanta Biologicals, Lawrenceville, GA, USA) and 1% penicillin/streptomycin (100 U/100 mg per mL; Gibco BRL), labeled complete media for simplicity. Cells were incubated at 37°C in 5% CO_2 with 100% humidity. Fibroblasts from 5 to 8 passages were used for all cell studies.

Morphometric Analysis of Fibroblast Growth on Scaffolds

Fibroblast morphology was characterized after 12, 48, and 96 hours of cell culture on scaffolds using fluorescent microscopy. Samples were rinsed twice with sterile phosphate-buffered saline (PBS) to remove nonattached debris. Cells were then fluorescently labeled with 20 mM rhodamine phalloidin to identify polymerized actin (Invitrogen) and 20 mM 4′,6-diamidino-2-phenylindole (DAPI) nuclear counterstain (Invitrogen) to identify the cell nucleus. Scaffolds were then rinsed in PBS to clear excess label. Cell fluorescence was preserved with Prolong Gold reagent (Invitrogen). Cell fluorescence and morphology were characterized at a magnification range from 10× to 40×.

Fibroblast Viability in Scaffold Cultures

Multiple methods were used to quantify cell adhesion and proliferation. Carbon and GJ scaffolds (area: 25 mm^2) were placed in 100-mm^2 round tissue culture dishes (n = 10 per experimental group). Fibroblasts (60,000 cells/sample) were seeded onto scaffold samples in 200-μL aliquots of F12 complete media containing 10% FBS (300,000 cells/mL) and placed into the incubator at 37°C, 5% CO_2, and 100% humidity. After 12 hours, samples were moved to 24-well plates, retaining only cells attached to the scaffolds, and 2 mL of complete media was added to each well and returned to the incubator. Growth media were changed every second day. Scaffolds were immediately processed for biochemical characterization as described below to measure cell attachment. To characterize fibroblast proliferation, cell-seeded scaffolds were cultured in 2 mL of complete media for a period of 12, 48, and 96 hours before analysis.

Cell attachment and proliferation was quantified with fluorescence microscopy and the WST-1 biochemical assay (Roche Scientific, Indianapolis, IN, USA) cultured for 12, 48, and 96 hours. Cell adhesion to scaffold surfaces was quantified by counting cell nuclei labeled with DAPI at each culture time point. For each scaffold, 5 images were acquired, spanning the entire length of the sample. Fibroblasts were imaged and nuclei were counted using the Metamorph software package (Molecular Devices, Sunnyvale, CA, USA).

Concurrently, cell viability was assessed at 12, 48, and 96 hours using WST-1 assay. The tetrazolium salt 2-(4-iodophenyl)-3-(4-nitrophenyl)-5-(2,4-disulfophenyl)-2H-tetrazolium, better known as WST-1, was used to quantify viable fibroblasts in culture. Photometric quantification of viable cells was performed by measuring absorbance at 450 nm and 690 nm using a microplate reader. Cell proliferation was measured as a function of absolute absorbance values (absorbance at 450 nm − absorbance at 690 nm). Fibroblast growth in wells without scaffolds was used as a positive control while scaffolds without seeded cells were used as negative controls. Nonspecific absorbance from media and scaffold samples was subtracted from absorbance readings. Absorbance values were compared with control values and related directly to cell viability.

Statistical Analysis

Statistical analyses were performed using the SPSS Statistics 19 Software Package (SPSS, Inc, Chicago, IL, USA). All experimental results were statistically evaluated using 1-way analysis of variance, with $P<.05$ indicating significant differences among experimental groups. Post hoc multiple comparison analyses were also performed using the Tukey-Kramer test. Multivariate stepwise linear regression was carried out to model the relationship between experimental parameters (porosity, elastic modulus, stress, and thickness) and load failure of carbon scaffolds and GJ. In addition, linear regression was performed to model the relationship between scaffold porosity and elastic modulus. Carbon samples were pooled for an n = 40. GJ data were also pooled for data analysis for n = 20.

RESULTS

Scaffold Characterization

As shown in Fig. 1, at low magnification (2×), all samples demonstrated porous characteristics; however, GJ was less porous than carbon scaffolds (see Fig. 1), which was most apparent on ESEM imaging shown in Fig. 2. GJ also displayed 2 distinct textured sides that relate to the natural stratification of structures in the human dermis

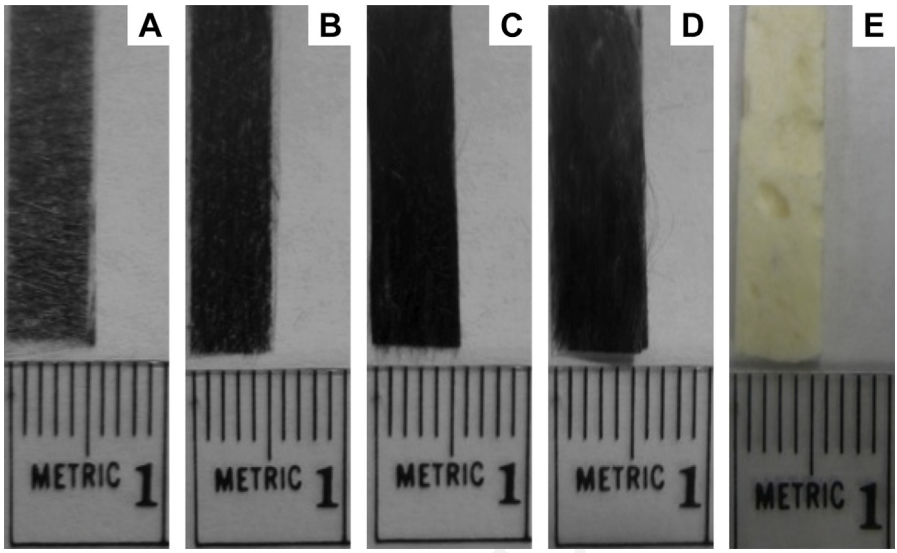

web 4C/FPO

Fig. 1. ■ Q10

(see Fig. 2). The deeper dermal side was characterized by an extensive vascular network and was more porous than the more superficial epidermal side of GJ control. GJ demonstrated less continuity and consistency in physical characteristics than engineered carbon, in accordance with natural variations typically observed in living tissues (Table 1) but not observed with highly engineered scaffolds such as carbon (see Fig. 1). Microscale porosity was examined in all scaffolds by μCT (see Fig. 2). Scaffold porosity was most uniform in carbon-engineered scaffolds, whereas GJ demonstrated inconsistent porosity attributes hallmarked by regions of large defects up to 1 mm in size that were not observed in any carbon-engineered scaffolds (see Fig. 2). GJ displayed a closed porosity of (35%), whereas carbon scaffolds showed an open cell structure (CF1 and CF2: 55% and 70%, respectively; CV1 and CV2: 80% and 95%, respectively) (see Fig. 2, Table 2). Structural characterization of scaffolds demonstrated less variability in porosity of carbon scaffolds compared with GJ, as indicated by smaller average standard deviations in porosity measurements. The standard deviation of carbon scaffold porosity was approximately 75% smaller than that of GJ (see Table 2). CF1 and CF2 exhibited greater unidirectional fiber orientation, whereas CV1 and CV2 scaffolds consisted of more randomly organized fibers (see Fig. 2; Fig. 3). Q8

Mechanical Behavior of Carbon Scaffolds

The mechanical properties of scaffolds were tested under tension. As shown in the magnified low strain range (0%–3%), GJ samples displayed a smaller stress-strain ratio than carbon-based scaffolds (Fig. 4). This finding is consistent with deformation characteristics commonly observed in the "toe region" of biological tissues. Furthermore, as is displayed by the gradual decrease in the slope of the curve, GJ exhibited longer strain regions with a yielding behavior and no catastrophic failure (see Fig. 4). Conversely, carbon scaffolds carried more load and handled a larger stress at lower strain, and failed catastrophically. From a load-failure perspective, CF1 displayed

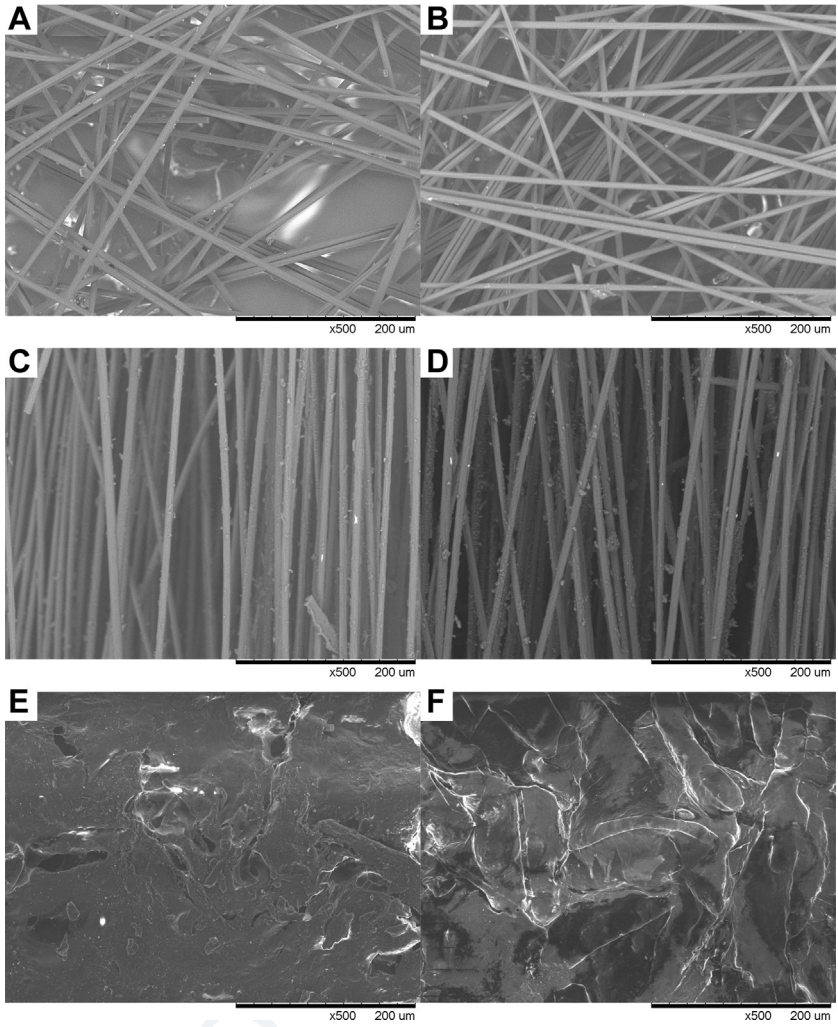

Fig. 2. ■

Table 1
Mechanical properties of living tissue Q11

	Maximum Load (N)	Maximum Stress (MPa)	Maximum Strain (%)	Elastic Modulus (MPa)
Femur[a]	111.0 ± 11.9	131 ± 13	5.00 ± 1.2	16,600 ± 174
Anterior cruciate ligament[b]	1627 ± 491	26.8 ± 9.1	28.5 ± 9.1	109.00 ± 50.0
Superior infraspinatus tendon[c]	462.8 ± 237	14.6 ± 7.7	Not reported	120.00 ± 53.1

[a] Fung Y. Biomechanics: mechanical properties of living tissues. Springer-Verlag; 1993. Q12
[b] Holzapfel G, Ogden R. Mechanics of biological tissue. Springer; 2006.
[c] Halder A, Zobitz ME, Schultz F, et al. Mechanical properties of the posterior rotator cuff. Clin Biomech (Bristol, Avon) 2000;15:456–62.

Table 2
Comparison of carbon scaffolds with GraftJacket scaffold

	Density (g/cm^3)	Porosity (%)	Thickness (mm)	Maximum Load (N)	Maximum Stress (MPa)	Maximum Strain (%)	Elastic Modulus (MPa)
Carbon veil 1 (CV1)	0.50	95 ± 1.0**	0.30 ± 0.03	3.0 ± 0.20**	2.5 ± 0.10***	3.3 ± 0.20***	860 ± 45**
Carbon veil 2 (CV2)	0.60	80 ± 4.0**	0.32 ± 0.02	4.0 ± 0.20**	3.2 ± 0.20***	2.5 ± 0.20***	910 ± 47**
Carbon fabric 1 (CF1)	0.80	55 ± 9.0	0.43 ± 0.03	56 ± 4.0*	21 ± 0.90**	2.3 ± 0.10**	995 ± 83**
Carbon fabric 2 (CF2)	0.70	70 ± 7.0*	0.42 ± 0.03	27 ± 3.0*	16 ± 1.0	2.7 ± 0.20**	835 ± 66**
GraftJacket Matrix (GJ)	1.1–1.4	35 ± 20	0.48 ± 0.14	36 ± 16	15 ± 2.5	49 ± 13	80 ± 19

Values with asterisks are significantly different from GJ: *$P \leq .05$; **$P \leq .005$; ***$P < .001$.

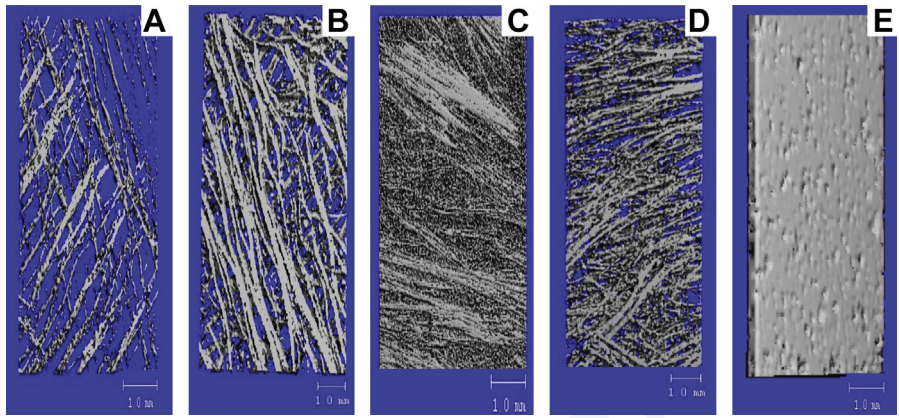

Fig. 3. ■

the greatest strength, with a maximum load of 56 ± 4 N, significantly greater than other carbon scaffolds and the GJ control. CF2 and GJ were most similar (27 ± 4 vs 36 ± 16 N), without statistically significant differences in load failure (P>.05) (Fig. 5, see Table 2). On the other hand, CV1 and CV2 scaffolds exhibited significantly lower

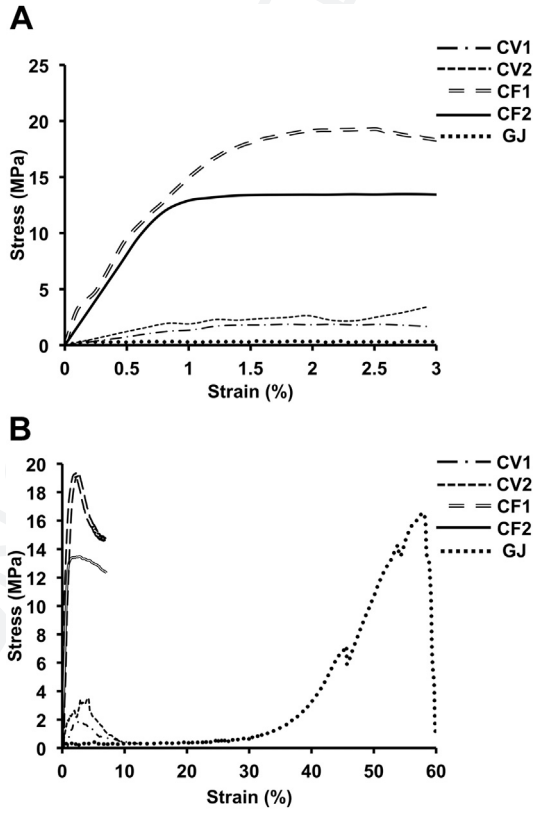

Fig. 4. ■

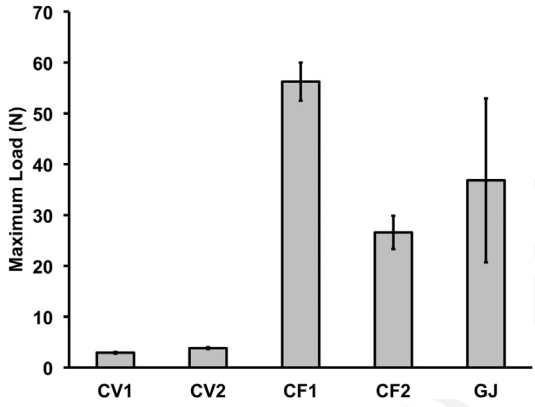

Fig. 5. ■

($P = .01$) maximum loads (3 ± 0.2 and 4 ± 0.2 N), than both CF scaffolds and the GJ control (see Fig. 5, Table 2). Results also showed that CF1 displayed a significantly greater ($P = .005$) maximum stress (21 ± 0.9 MPa) in comparison with the GJ control (15 ± 2.5 MPa) (Fig. 6, see Table 2). The variability of load failure and porosity was

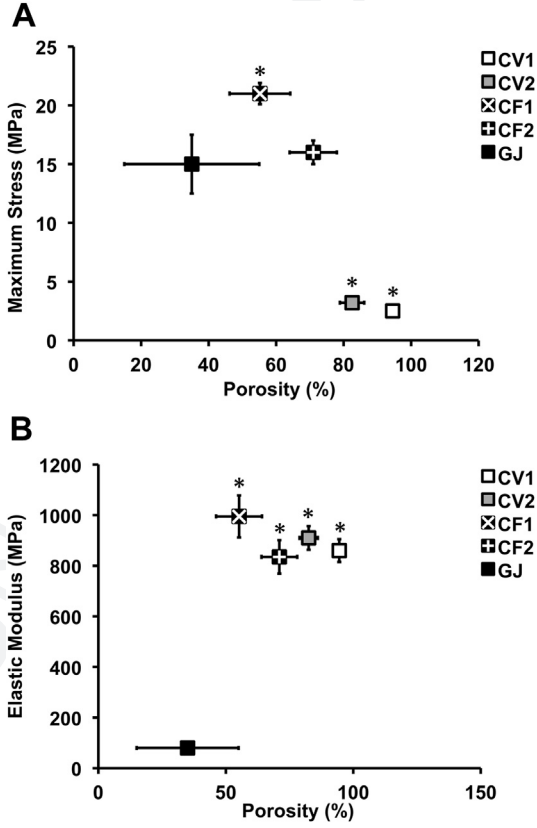

Fig. 6. ■

much greater in GJ than in engineered carbon scaffolds, as demonstrated by higher standard deviations of test measurements. In addition, all carbon-engineered scaffolds (CV1, CV2, CF1, and CF2) displayed significantly greater ($P = .005$) elastic modulus values (860 ± 45, 910 ± 47, 995 ± 83, and 835 ± 66 MPa, respectively) than the GJ control (see Fig. 6, Table 2).

Cytoskeletal Actin Polymerization and Morphology of Fibroblasts Cultured on Carbon Scaffolds

Cell density and morphology of fibroblasts cultured on scaffolds were characterized using fluorescent microscopy (Fig. 7). Actin filament organization was most distinct in elongated fibroblasts, which grew in a collinear pattern along carbon fibers. This pattern of fibroblast growth was most prevalent in CV, which was notably more porous than other tested scaffolds. Actin polymerization was diffuse and without distinct actin filament formation in fibroblasts with a round morphology and in fibroblasts observed in clusters. This pattern of morphology was most prevalent in regions of dense carbon fiber arrangement more frequently observed in CF than in CV where CF fibers were arranged in a tightly packed parallel alignment (see Fig. 2). Although round and elongated fibroblast morphology was observed in all scaffolds, predominant patterns of morphology suggest that cell aggregation and round morphology may be more related to the density of carbon fiber distribution rather than differences between parallel and divergent fiber orientation within carbon scaffolds.

Cell adhesion and proliferation exhibited 2 distinct growth patterns in GJ controls that were specific to the epidermal and dermal surfaces of GJ. The dermal surface of GJ supported cell adhesion and growth with extensive filamentous actin organization in fibroblasts, while the epidermal surface supported minimal actin polymerization in fibroblasts (see Fig. 7). The morphology of fibroblast adhesion and growth on CF scaffolds closely resembled that of fibroblast adhesion to the epidermal surface of GJ controls where extensive actin polymerization could be identified in fibroblasts (see Fig. 7). The morphology of fibroblast adhesion to CV scaffolds more closely resembled fibroblast adhesion to the dermal surface of GJ controls (see Fig. 7).

Fibroblast Adhesion and Proliferation on Carbon Scaffolds

Cell density and viability assays were conducted to assess fibroblast growth and proliferation on carbon scaffolds. The cell density of fibroblasts cultured on scaffolds for periods of 12, 48, and 96 hours was determined using Metamorph counting software. Fibroblast adhesion and proliferation on CF and CV scaffolds was significantly lower than growth on GJ controls ($P<.01$) (Fig. 8). Total fibroblast adhesion to CF1 was significantly greater than that in CV scaffolds ($P = .005$) (see Fig. 8). There were significant differences in cell adhesion ($P = .01$) and proliferation ($P = .005$) between CF1 and CF2 scaffold cultures. Furthermore, there was a positive proportional trend in fibroblast adhesion to scaffolds with lower porosity (see Fig. 8).

WST-1 analysis demonstrated marginal differences in fibroblast viability and proliferation on carbon and GJ control scaffolds during the first 12 hours of culture; however, significantly higher WST-1 absorbance was measured in dermal control cultures at 96 hours, which suggests that carbon scaffolds were less capable of supporting a high rate of cell proliferation over time ($P = .01$). At 96 hours, CF was most similar to GJ controls in sustaining fibroblast growth, with CF1 and CF2 demonstrating 16% and 27% less absorbance than GJ controls. By contrast, CV scaffolds showed notably lower capacity to support cell growth than GJ, with 80% and 77% less absorbance on CV1 and CV2.

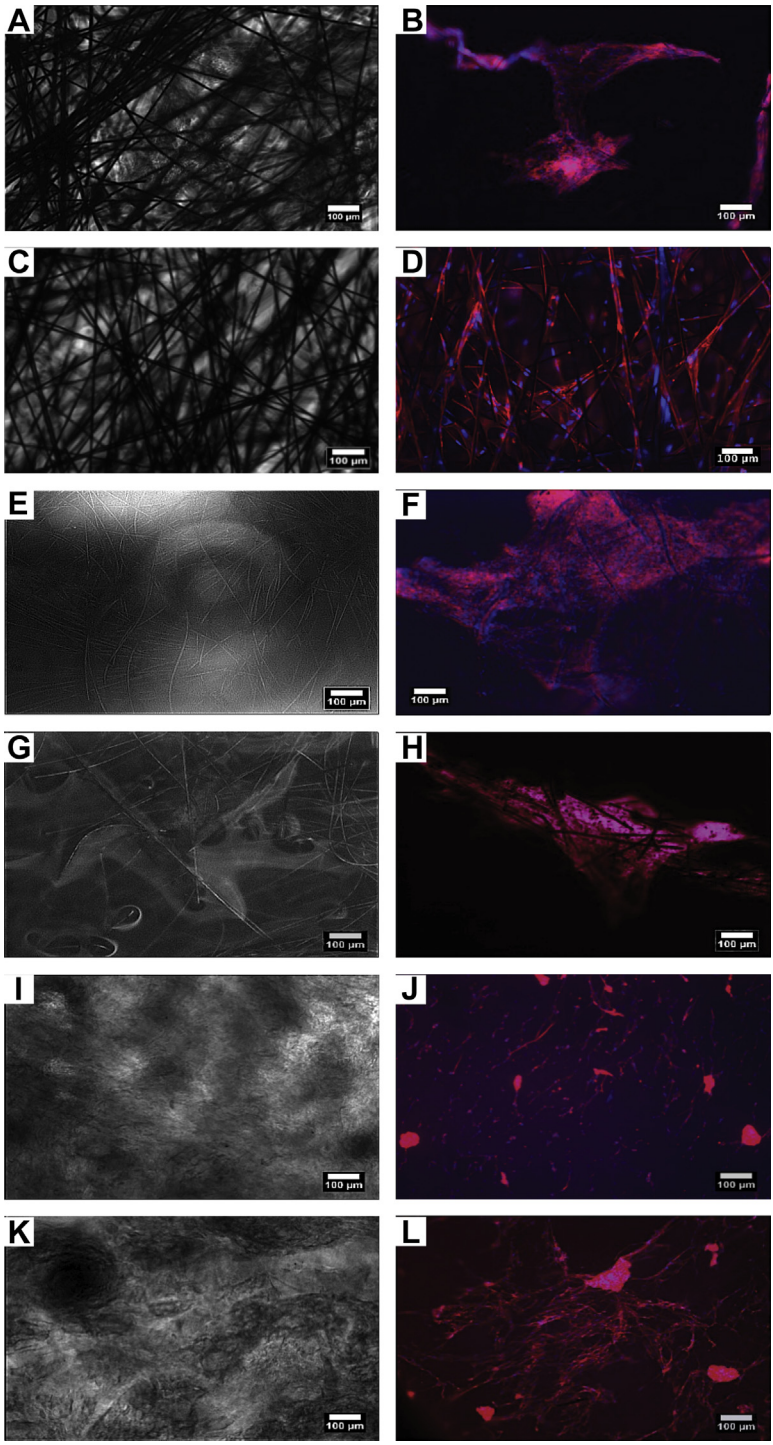

Fig. 7. ■

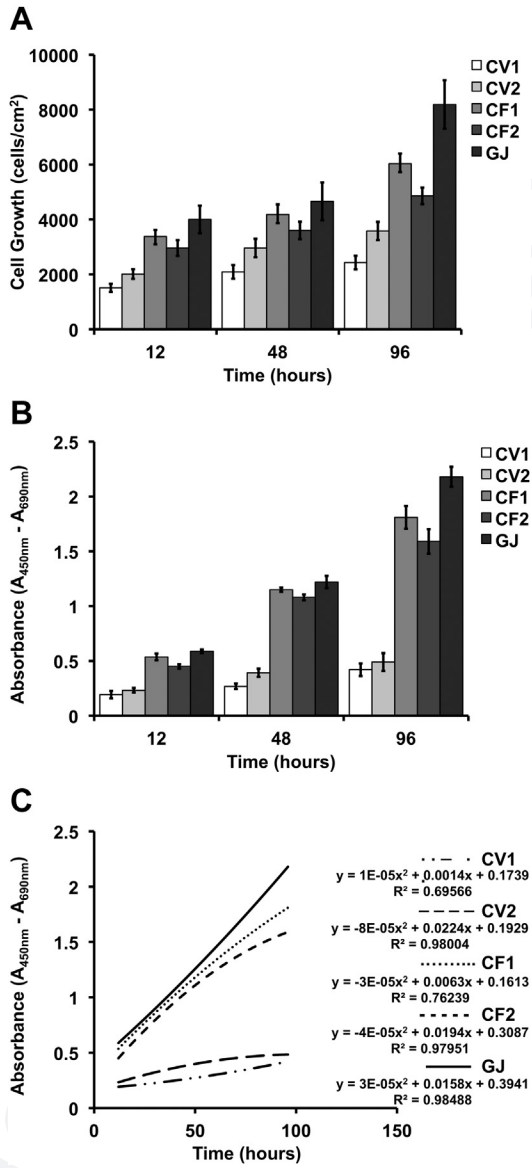

Fig. 8. ■

Multivariate Stepwise Regression

Stepwise regression analysis demonstrated that scaffold thickness and porosity accounted for significant variability in load failure of GJ (adjusted R^2 = 0.787 and 0.924, respectively) but not carbon scaffolds (Fig. 9). The variability in load failure of carbon scaffolds was more closely related with modulus and stress properties of carbon (Adjusted R^2 = 0.924). In addition, linear regression analysis revealed that porosity did not strongly correlate with elastic modulus in both control and carbon scaffold groups (adjusted R^2 = 0.087 and 0.383, respectively) (Fig. 10).

A

Variable	B	SE B	β
Step 1			
Stress	2.55	0.117	0.962*
Step 2			
Stress	2.35	0.077	0.886*
Modulus	0.059	0.008	0.229*

Note. $R^2 = 0.926$ for Step 1; Adj. $R^2 = 0.924$ for Step 1, $R^2 = 0.972$ for Step 2, Adj. $R^2 = 0.971$ for Step 2, (*P<.01). Porosity and thickness were removed due to significance test (P>.05).

B

Variable	B	SE B	β
Step 1			
Porosity	- 1.15	0.383	- 0.690*
Step 2			
Porosity	- 1.28	0.234	- 0.764**
Thickness	22.8	5.35	0.596**

Note. $R^2 = 0.476$ for Step 1; Adj. $R^2 = 0.423$ for Step 1, $R^2 = 0.826$ for Step 2, Adj. $R^2 = 0.787$ for Step 2, (*P<.05, **P<.01). Stress and elastic modulus were removed due to significance test (P>.05).

Fig. 9. ■

A

Variable	B	SE B	β
Porosity	- 3.42	0.681	- 0.631*

Note. $R^2 = 0.399$; Adjusted $R^2 = 0.383$ (*P<.001).

B

Variable	B	SE B	β
Porosity	- 0.409	0.286	- 0.412

Note. $R^2 = 0.170$; Adjusted $R^2 = 0.087$ (P>.05).

Fig. 10. ■

DISCUSSION

Carbon has previously been used in a limited capacity in medical implants used for soft-tissue augmentation.[26,27,30,33,34] In the past, researchers have combined biopolymers[35–37] and have altered the surface chemistry[38] of materials to optimize the biocompatibility and function of scaffolds. The use of fibrous carbon materials for medical research has steadily grown as processing and characterization methods have become more sophisticated, allowing precise tuning of physical and structural properties of carbon-based scaffolds on a nanoscale. The objective of this study was to investigate the potential use of carbon as a biomedical scaffold for the surgical reconstruction of soft tissues, with a hypothesis that carbon may provide an optimal balance of biomechanical strength and the capacity to deliver living cells and biologics to surgical sites to promote tissue repair while restoring tissue function. This study demonstrated that carbon may support biological functions in addition to serving biomechanical functions as a material known for its biocompatibility, durability, and strength.

Cell adhesion and proliferation studies showed that there is little difference between carbon and GJ's capacity to support early cell adhesion, a critical factor for scaffold integration and healing in vivo. This finding is supported by marginal differences in fibroblast density and viability on both carbon and control scaffolds during short-term in vitro cultures at 12 hours and up to 48 hours in CF cultures. The capacity for carbon to sustain fibroblast adhesion and viability at 96 hours' culture suggests a potential use of carbon as a scaffold for sustained delivery of growth factors to sites of injury to promote tissue healing, such as the commercially available scaffold Apligraft, which is composed of a collagen scaffold seeded with keratinocytes and dermal fibroblasts.[24] Fibroblast adhesion to carbon and the capacity to sustain cell growth are critical factors for the use of carbon as a vehicle for delivering viable cells to a region of soft-tissue reconstruction where the combination of cells and scaffold are a source of extracellular matrix synthesis, paracrine release of growth factors, and nidus for tissue repair.

Although fibroblast adhesion to carbon and GJ was followed by cell proliferation, proliferation was slower on carbon scaffolds, as demonstrated by fewer cells and less metabolic activity measured by WST-1 assays in longer-term cultures of 96 hours. These findings suggest significant biological property differences between carbon and the tissue-derived GJ. These differences yielded a higher rate of fibroblast proliferation on GJ than on carbon. It is reasonable to speculate that enhanced fibroblast proliferation on GJ was stimulated by residual activities of growth factors such as basic fibroblast growth factor, which has been shown to be retained in GJ but not to be present in carbon.[6] Hence carbon's limited potential in supporting a high rate of cell proliferation may be due to its lack of a naturally derived tissue factor found in GJ. Further investigation of the specific role of growth factors present in GJ and selective conjugation of growth factors to carbon scaffolds may be necessary to optimize carbon's potential to promote cell proliferation to levels observed with tissue scaffolds used in surgery today. Recent studies have shown that some synthetic fiber scaffolds can be modified to mimic the activity of specific growth factors such as vascular endothelial growth factor and to promote regenerative processes such as neovascularization.[39] This option may offer an alternative approach to growth factor conjugation to carbon that improves the biological potential of carbon as a regenerative scaffold.

It is unlikely that lower rates of fibroblast proliferation on carbon scaffolds was due to carbon toxicity, as carbon has been shown to be nontoxic in itself[17,27,33,40,41] and progressive cell proliferation would not be expected as observed if carbon was

cytotoxic. Lower levels of total fibroblast adhesion to carbon scaffolds than to GJ may have been a result of geometric differences in the design and structure of carbon and GJ scaffolds. CV, the more porous of the 2 carbon scaffolds, demonstrated less capacity for cell adhesion and lower proliferation rates, as noted by a smaller plateau in WST-1 absorbance and lower levels of cell adhesion than carbon fabric and GJ. This finding is consistent with other studies that demonstrate increased cell proliferation on less porous scaffolds and densely organized regions of carbon fiber organization.[42] These findings are also consistent with literature regarding cell proliferation on synthetic fibers, in which cell proliferation was greatest in regions of cell aggregation and spreading.[41,43,44] The carbon fiber used in this study had a high degree of basal planes oriented along the fiber axis. The basal planes are formed during the carbonization step of carbon fiber processing. After carbonization, the fibers exhibit a high degree of axial preferred orientation with thick crystallite stacking. As shown in **Fig. 7**, there was high actin polymerization along the fiber axis. This material property has been previously shown to promote cell growth.[33,45] The optimal pattern of fiber organization, dimension, and porosity that maximizes the ability of carbon to deliver cells, promote tissue repair, and enable tissue ingrowth and neovascularization needs to be further explored.

In the past, it has been exceptionally challenging to engineer synthetic scaffolds or to process naturally derived tissues to recapitulate the biological parameters necessary for tissue repair without compromising the mechanical strength and stiffness of scaffolds. This problem is a particularly keen one with scaffolds used to repair major tendon injuries of the rotator cuff or Achilles tendon, where dermal scaffolds currently used to augment tissue repair are composed of similar extracellular matrix molecules but fail to restore the elastic properties of tendons.[10,12,14,46–48] Regression modeling demonstrated that scaffold porosity, a major factor influencing graft neovascularization and cell-delivery capacity of fibrous scaffolds, did not significantly influence the load failure and modulus of carbon but did influence variance in load failure of GJ. These findings suggest design advantages of carbon scaffold engineering that maximize porosity attributes conducive to scaffold neovascularization, without compromising the mechanical strength of a scaffold that is needed but often lacking in currently available products. The results of this study demonstrated greater consistency, less variation, and fewer defects in the dimensions, porosity, and thickness of engineered carbon than the commercially available GJ (see **Fig. 6**). The ability to consistently manufacture precise physical and dimensional properties of carbon may further minimize design, biomechanical, and manufacturing limitations of current scaffolds used in surgery. Hence, achieving the optimal tunable balance between biological properties and biomechanical function of scaffolds may be technically easier through carbon engineering than by developing improved technologies of human tissue processing. The possibility of engineering carbon with mechanical properties of a mature tissue, despite its lack of a mature cellular and extracellular matrix, provides a potential advantage of carbon over current biological scaffolds that require prolonged processes of tissue healing, reorganization, and fibrosis to achieve their maximum mechanical strength. This advantage potentially shortens periods of postoperative inactivity in patients, as the mechanical strength of tendons repaired with carbon may be restored sooner with surgery without the need for prolonged periods of immobilization to achieve maximal tissue strength. This approach may ultimately reduce the risk of postoperative morbidity and mortality associated with prolonged periods of inactivity and immobilization by enabling patients to return to unrestricted activities earlier.[49,50]

In vitro studies have been the first stepping-stone in biological explorations. However, to complement such explorations, researchers have looked toward

computational programs to determine efficacy or performance. Finite element analysis has long been used as a computational method to determine failure criteria of designs, for example, in understanding flow and strength in structures used as blood vessel replacements. In the current study, cellular automata are explored as a method to investigate cellular response. It would greatly benefit researchers to understand response by executing a program and analyzing the results. The implication of computational technology in biological studies is enormous. This study has been able to show that 3-dimensional models may help understand the attachment, growth, and proliferation of cells on carbonaceous materials. However, this model may also be expanded to incorporate other types of materials. The model indicated that the attachment and growth of osteoblasts was initially on carbon materials. However, most growth was around the intersection of carbon materials; this may be a key factor in designing scaffolds with optimized architecture. The optimum distance and orientation for cellular movement across ligaments may be analyzed by modifying the model parameters. In addition, cells seemed to proliferate from these intersections and across carbon fibers. Increasing the immediate surface area of scaffold material may support greater cell attachment, movement, and overall growth. Whereas the current model only integrated 3 parameters, incorporating other parameters such as surface roughness, surface charge, or fiber orientation may strengthen a future model.

SUMMARY

Carbon may represent an alternative material suitable for future development as a soft-tissue substitute that potentially optimizes the biological and mechanical properties required for a graft product used in surgery. In addition, other modes of characterization such as 3-dimensional computational modeling may offer an insight into material performance in a biological environment. Further investigation is required to characterize and model the relationships between biological, mechanical, and design properties of this material to maximize its potential as a biomechanical scaffold and vehicle for delivering biologics that promote tissue repair and regeneration.

REFERENCES

1. Sheridan RL, Choucair RJ. Acellular allogenic dermis does not hinder initial engraftment in burn wound resurfacing and reconstruction. J Burn Care Rehabil 1997;18:496.
2. Sikka RS, Narvy SJ, Vangsness CT. Anterior cruciate ligament allograft surgery underreporting of graft source, graft processing, and donor age. Am J Sports Med 2011;39:649.
3. Azar FM. Tissue processing: role of secondary sterilization techniques. Clin Sports Med 2009;28:191.
4. Cornwell KG, Landsman A, James KS. Extracellular matrix biomaterials for soft tissue repair. Clin Podiatr Med Surg 2009;26:507.
5. Billiar K, Murray J, Laude D, et al. Effects of carbodiimide crosslinking conditions on the physical properties of laminated intestinal submucosa. J Biomed Mater Res 2001;56:101.
6. Valentin JE, Badylak JS, McCabe GP, et al. Extracellular matrix bioscaffolds for orthopaedic applications—a comparative histologic study. J Bone Joint Surg Am 2006;88A:2673.
7. Bjork JW, Johnson SL, Tranquillo RT. Ruthenium-catalyzed photo cross-linking of fibrin-based engineered tissue. Biomaterials 2011;32:2479.

8. Scutt N, Rolf CG, Scutt A. Tissue specific characteristics of cells isolated from human and rat tendons and ligaments. J Orthop Surg Res 2008;3:32.
9. MacLeod TM, Williams G, Sanders R, et al. Prefabricated skin flaps in a rat model based on a dermal replacement matrix Permacol (TM). Br J Plast Surg 2003;56:775.
10. Barber FA, McGarry JE, Herbert MA, et al. A biomechanical study of Achilles tendon repair augmentation using GraftJacket matrix. Foot Ankle Int 2008;29:329.
11. Snyder SJ, Arnoczky SP, Bond JL, et al. Histologic evaluation of a biopsy specimen obtained 3 months after rotator cuff augmentation with GraftJacket matrix. Arthroscopy 2009;25:329.
12. Lee DK. A preliminary study on the effects of acellular tissue graft augmentation in acute Achilles tendon ruptures. J Foot Ankle Surg 2008;47:8.
13. Wong I, Burns J, Snyder S. Arthroscopic GraftJacket repair of rotator cuff tears. J Shoulder Elbow Surg 2010;19:104.
14. Ozaki J, Fujimoto S, Masuhara K, et al. Reconstruction of chronic massive rotator cuff tears with synthetic materials. Clin Orthop Relat Res 1986;202:173.
15. Brown BN, Barnes CA, Kasick RT, et al. Surface characterization of extracellular matrix scaffolds. Biomaterials 2010;31:428.
16. Asran AS, Henning S, Michler GH. Polyvinyl alcohol-collagen-hydroxyapatite biocomposite nanofibrous scaffold: mimicking the key features of natural bone at the nanoscale level. Polymer 2010;51:868. Q9
17. Demmer P, Fowler M, Marino AA. Use of carbon-fibers in the reconstruction of knee ligaments. Clin Orthop Relat Res 1991;271:225.
18. Cornwell KG, Pins GD. Enhanced proliferation and migration of fibroblasts on the surface of fibroblast growth factor-2-loaded fibrin microthreads. Tissue Eng Part A 2010;16:3669.
19. Cooper JA, Lu HH, Ko FK, et al. Fiber-based tissue-engineered scaffold for ligament replacement: design considerations and in vitro evaluation. Biomaterials 2005;26:1523.
20. Freeman JW, Woods MD, Cromer DA, et al. Evaluation of a hydrogel-fiber composite for ACL tissue engineering. J Biomech 2011;44:694.
21. Tay BY, Zhang SX, Myint MH, et al. Processing of polycaprolactone porous structure for scaffold development. J Mater Proc Tech 2007;182:117.
22. Rush SM, Hamilton GA, Ackerson LM. Mesenchymal stem cell allograft in revision foot and ankle surgery: a clinical and radiographic analysis. J Foot Ankle Surg 2009;48:163.
23. McKay W, Peckham S, Badura J. A comprehensive clinical review of recombinant human bone morphogenetic protein-2 (INFUSE® Bone Graft). Int Orthop 2007; 31:729.
24. Falanga V, Sabolinski M. A bilayered living skin construct (APLIGRAF®) accelerates complete closure of hard-to-heal venous ulcers. Wound Repair Regen 1999;7:201.
25. Takaseya T, Fumoto H, Shiose A, et al. In vivo biocompatibility evaluation of a new resilient, hard-carbon, thin-film coating for ventricular assist devices. Artif Organs 2010;34:1158.
26. Chen L, Yuan XB, Sun HW, et al. In vivo study of carbon artificial femoral head. High-Performance Ceramics 2010;434–435:613.
27. Cao N, Wang QX, Dung JW, et al. Characterization and biological behavior of a carbon fiber/carbon composite scaffold with a porous surface for bone tissue reconstruction. New Carbon Mater 2010;25:232.
28. Kettunen J, Makela A, Miettinen H, et al. Fixation of distal femoral osteotomy with an intramedullary rod: early failure of carbon fibre composite implant in rabbits. J Biomater Sci Polym Ed 1999;10:715.

29. Hilder TA, Hill JM. Carbon nanotubes as drug delivery nanocapsules. Curr Appl Phys 2008;8:258.
30. Bianco A, Kostarelos K, Prato M. Applications of carbon nanotubes in drug delivery. Curr Opin Chem Biol 2005;9:674.
31. Martin BR, Sangalang M, Wu S, et al. Outcomes of allogenic acellular matrix therapy in treatment of diabetic foot wounds: an initial experience. Int Wound J 2005; 2:161.
32. Liden BA, Simmons M. Histologic evaluation of a 6-month GraftJacket matrix biopsy used for Achilles tendon augmentation. J Am Podiatr Med Assoc 2009;99:104.
33. Czarnecki JS, Lafdi K, Tsonis PA. A novel approach to control growth, orientation, and shape of human osteoblasts. Tissue Eng Part A 2008;14:255.
34. Baquey C, Bordenave L, More N, et al. Biocompatibility of carbon-carbon materials: blood tolerability. Biomaterials 1989;10:435.
35. Edwards SL, Werkmeister JA, Ramshaw JA. Carbon nanotubes in scaffolds for tissue engineering. Expert Rev Med Devices 2009;6:499.
36. Fu T, Zhao JL, Wei JH, et al. Preparation of carbon fiber fabric reinforced hydroxyapatite/epoxy composite by RTM processing. J Mater Sci 2004;39:1411.
37. Hirata E, Uo M, Takita H, et al. Development of a 3D collagen scaffold coated with multiwalled carbon nanotubes. J Biomed Mater Res B Appl Biomater 2009;90B: 629.
38. Chu PK. Enhancement of surface properties of biomaterials using plasma-based technologies. Surf Coat Tech 2007;201:8076.
39. Igarashi S, Tanaka J, Kobayashi H. Micro-patterned nanofibrous biomaterials. J Nanosci Nanotechnol 2007;7:814.
40. Price RL, Ellison K, Haberstroh KM, et al. Nanometer surface roughness increases select osteoblast adhesion on carbon nanofiber compacts. J Biomed Mater Res A 2004;70A:129.
41. Morris DM, Hindman J, Marino AA. Repair of fascial defects in dogs using carbon fibers. J Surg Res 1998;80:300.
42. Desai VV, Newman JH. The histology of regenerated tissue after failed carbon fibre matrix implants. Knee 1999;6:229.
43. Rajzer I, Menaszek E, Bacakova L, et al. In vitro and in vivo studies on biocompatibility of carbon fibres. J Mater Sci Mater Med 2010;21:2611.
44. Rnjak J, Li Z, Maitz PK, et al. Primary human dermal fibroblast interactions with open weave three-dimensional scaffolds prepared from synthetic human elastin. Biomaterials 2009;30:6469.
45. Bacakova L, Svorcik V, Rybka V, et al. Adhesion and proliferation of cultured human aortic smooth muscle cells on polystyrene implanted with N^+, F^+ and Ar^+ ions: correlation with polymer surface polarity and carbonization. Biomaterials 1996;17:1121.
46. Lee DK. Achilles tendon repair with acellular tissue graft augmentation in neglected ruptures. J Foot Ankle Surg 2007;46:451.
47. Branch JP. A tendon graft weave using an acellular dermal matrix for repair of the Achilles tendon and other foot and ankle tendons. J Foot Ankle Surg 2011;50:257.
48. Derwin KA, Codsi MJ, Milks RA, et al. Rotator cuff repair augmentation in a canine model with use of a woven poly-L-lactide device. J Bone Joint Surg Am 2009;91A: 1159.
49. Cogo A, Bernardi E, Prandoni P, et al. Acquired risk factors for deep-vein thrombosis in symptomatic outpatients. Arch Intern Med 1994;154:164.
50. Roberts CS, Ojike NI, Bhadra AK, et al. Venous thromboembolism in shoulder surgery: a systematic review. Acta Orthop Belg 2011;77:281.